FINDING SPECIFIC SPECTRAL FEATURES FOR SURFACE-ENHANCED RAMAN RESPONSE OF *ENTEROCOCCUS FAECALIS* ASSISTED BY MULTIVARIATE ANALYSIS WHEN USING COMMON SILVER SOLS

L. STĂNCIOIU[1], A.M.R. GHERMAN[1,2], N.E. DINA[2*]

[1]Faculty of Physics, Babeș-Bolyai University,
1 Kogălniceanu, RO-400084, Cluj-Napoca, Romania
E-mail: laurentiu.stancioiu@gmail.com

[2]Department of Molecular and Biomolecular Physics, National Institute for R&D of Isotopic and Molecular Technologies,
67-103 Donat, RO-400293, Cluj-Napoca, Romania
E-mail: raluca.gherman@itim-cj.ro *Email*: nicoleta.dina@itim-cj.ro (corresponding author)

Received Month 11, 2020

Abstract. Surface-enhanced Raman scattering (SERS) was employed for *Enterococcus faecalis* detection when using three common silver-based SERS-active sols. The SERS spectra obtained for the same species were compared in terms of bands' intensities and Raman shifting. By using multivariate analysis, the spectral data were classified depending on the sample preparation protocol.

Key words: multivariate analysis, *Enterococcus faecalis*, surface-enhanced Raman scattering.

1. INTRODUCTION

Surface-enhanced Raman scattering (SERS) is one of the most extensively used enhanced vibrational spectroscopies for bacteria detection and disease diagnosis. It combines the simple sample preparation and molecular specificity of Raman spectroscopy, its non-destructive nature and water obliviousness, with portable instrumentation and ultrasensitivity due to *localized surface plasmonic enhancement*. In Raman scattering the Stokes signal is proportional to the Raman cross section of the molecule, the number of molecules in the sample and the excitation laser intensity. In SERS, the Stokes Raman signal is proportional in addition to the number of molecules attached to a metallic nanostructures, offering huge enhancement [1]. The enhancement mechanism when using a SERS-active system, usually composed of metallic nanostructures, nanometer scaled with respect to the wavelength of the exciting light (the laser line), is generally attributed to the electromagnetic field (EF) enhancement through *localized surface plasmon*

resonance (LSPR) by a factor of 10^3-10^{11}. The introduction of the "*hot-spots*", as huge EF enhancement sites found at interstices between nanostructures is a consequence of the non-homogenous mixture of the colloidal solution, the aggregation causing difficult control on the size of the clusters, which is crucial for the enhancement [2].

SERS is a versatile, low-cost, non-destructive spectroscopic technique determining the molecular "fingerprint" of bioanalytes which competes with conventional molecular biology techniques and the omnipresent "omics" commonly used for infections diagnosis, for instance. SERS main advantages are the detection of low concentration bacteria, its selectivity due to spectroscopic fingerprinting of chemical and biological systems and the facile and fast preparation by simply mixing the colloid with the bacterial cells.

Two types of SERS approaches are largely used to detect bacteria. The label-based method requires a SERS-tag such as aptamers or antibodies which produce distinctive and ultra-sensitive signals. One drawback is the fact that the tags bind to the analyte which may cause interference in the characteristic SERS spectra. By contrast, label-free SERS detection does not need a specific label, hence, it provides direct informative characteristic spectra of bacterial pathogens found in the proximity of rough metal surfaces. One of the disadvantages to stumble across in label-free SERS detection can be the noise-to-spectra ratio, which can be overcome by selectivity and performant SERS-active substrates.

SERS has reached maturity as an analytical technique, but until now there has been no unitary approach that describes SERS experiments. The high potential for sample standardization is one of its main assets that will empower SERS as a fit-to-purposes modern technique with extensive use in clinical premises. A coherent sample pretreatment for biological material would simplify even more SERS-based biosensing applications and facilitate SERS entrance in daily clinical routines. Sols are most common and simple to use in "mix and try" sample preparation protocols. Silver sols (AgNPs) are more efficient when sensing bacteria since several chemical species found between the bacterial wall's components are prone to adsorb on the silver surface of intimately close nanostructures without linkers.

Enterococcus faecalis is a Gram-positive, commensal pathogen that usually inhabits the gastrointestinal tracts of humans and mammals [3]. *E. faecalis* is found in healthy humans, and actually helps the gastrointestinal microflora by its bacteriocin production, which has been investigated as a therapeutic agent. Some of its properties as the production of enterocin OE-342 indicates immunity enhancement and even anticancer potential [4]. Nevertheless, these bacteria can cause life-threatening infections due to their survival at pasteurization temperatures, high antibiotic resistivity [3] and rapid growth in normal conditions. Thus, the current drive to find a simple, non-invasive method of detecting this pathogen. However, the herein results are not focused on the pathogen's detection at trace levels, but

specifically, on how its spectral fingerprint might fluctuate under certain experimental conditions.

In this work, we exploit three experimental protocols in order to prove the specificity of label-free SERS approach as biosensing tool in bacteria detection and also to look into the spectral features that might intervene in bacteria barcoding when using different sols for sample preparation.

The three sols used are *in situ* synthesized [5] and *a priori* synthesized Leopold-Lendl [6] (LL) silver colloids and Lee-Meisel [7] colloid (LM). Subsequently, we used the *Principal Component Analysis* (PCA), as an unsupervised statistical chemometric technique for reducing the dimensionality of complex spectral datasets and determining the key variables in order to still be clinically relevant. This was achieved by keeping the SERS markers bands for bacterial barcoding in the major contributing principal components (PCs). *Linear Discriminant Analysis* (LDA) was used, additionally, for creating a classification model qualified to discriminate between the SERS signals of the same bacterial species but subjected to different sample preparation protocols and to identify unknown samples.

The main purpose of the article is to highlight the potential of data analysis to actually be able to discern between three different sample preparation protocols of the biomass, to spot the similarities and the differences between them when dealing with a real-life sampling.

2. EXPERIMENTAL

Enterococcus faecalis cultivation

For *bacterial cells activation,* aliquot with *E. faecalis* -stored at -80°C was previously partially thawed at room temperature. After thawing, 1 µL of bacteria was transferred using a sterile plastic loop into a new tube containing 5 mL of liquid Luria Broth (LB) media. The LB medium was previously sterilized by autoclaving at 121°C for 5 minutes. The tube containing media and the inoculum was vortexed for 5 seconds (max. speed) and then incubated overnight at 37°C. To obtain pure colonies, 10 µL from overnight culture was then subjected to serial dilution technique. After inoculation of LB medium with the desired dilution, the Petri dishes were incubated 15 minutes at room temperature and then were transferred to the incubator at 37°C overnight (at least 20 hours).

Standardized SERS samples preparation

After incubation, a single colony of bacteria was transferred into 5 ml of sterile LB Broth and grown overnight at 37°C. 4 mL of *E. faecalis* culture were centrifuged at 3000 x g for 2 minutes, the supernatant was discarded and the remained pellet was resuspended (washed) in 2 mL of sterile saline solution and gently vortexed. This washing protocol was repeated three times for a thorough discard of the media components. The working culture was obtained through resuspension of the obtained

pellet in 200 µL of sterile saline solution. For SERS testing, 100 µL bacterial solution was added to 900 µL of sol, obtaining a 10^8 cells/ml final concentration in each case.

Preparation of SERS-active AgNPs

Silver nanoparticles were synthesized to produce enhanced Raman signals using three different methods: *in situ*, where the exact protocol described in [5] was applied; Lee-Meisel synthesis by combining an aqueous solution of 10^{-3} mol $AgNO_3$ with a 1 mol solution of sodium citrate at boiling temperature and then magnetic stirring it for 20 minutes, obtaining a yellowish grey colloid. At last, the Leopold-Lendl colloid was prepared by dissolving 17 mg (0.1 mmol) $AgNO_3$ in 10 mL Milli-Q water. In a total volume of 100 mL, 11.6 mg (0.17 mmol) $NH_2OH{\cdot}HCl$ and 3.3 mL NaOH (0.1mol) were simply mixed with the silver nitrate solution, at room temperature. A greyish-brown sol was obtained.

SERS signal acquisition

SERS spectra were registered by using a portable BW-TEK *i*-Raman spectrometer coupled with a BW-TEK optical microscope through an optical fiber. The spectrometer is equipped with a 532 nm laser line having a total power of 50mW. The microscope was used with a 20× objective (N.A. 0.4, D=12 mm).

At least 15 spectra were recorded for each sample, as standardized cultures were used in triplicates. By qualitatively analyzing the SERS bands' intensity, in terms of counts recorded with a threshold of minimum 500 counts, nine spectra were selected for each situation: *in situ* synthesized (*in situ*) and *a priori* synthesized AgNPs using the Leopold-Lendl (LL) and Lee-Meisel (LM) method. The acquisitions were made with an exposure time of 25 seconds, multiplied 4 times, by using the long working objective (20×) and 5µl sample droplet from wet to dry conditions. All SERS 27 signals are plotted in Fig. 1 together with a mean spectrum for each dataset.

3. COMPUTATIONAL

The multivariate analyses were performed by using The Unscrambler X software version 10.4 developed by CAMO. Before database gathering, we performed baseline correction on all spectra by choosing the adaptive option, with zero offset and a coarseness of 21% in SpectraGryph (Friedrich Menges, 2001-2018). We used the same software to obtain the average spectra plotted in Fig. 1 (coloured) as a mean of all acquisitions. All SERS spectra are plotted in Origin (OriginLab, Northampton, MA). Fig. 2, 3 and 4 are loadings, 3D scores, respectively discrimination plots exported from The Unscrambler.

4. RESULTS AND DISCUSSION

It is assumed that operating conditions can affect the bacterial physiological state and their metabolic activity, causing also fluctuations in the SERS fingerprint [8, 9]. As it can be observed in Fig. 1 the recorded SERS fingerprint of *E. faecalis* is highly reproducible and stable in terms of bands' intensities and Raman shifting for all three sample protocols. The main SERS marker bands present in all spectra depicted are 728 cm^{-1} and 1321 cm^{-1}.

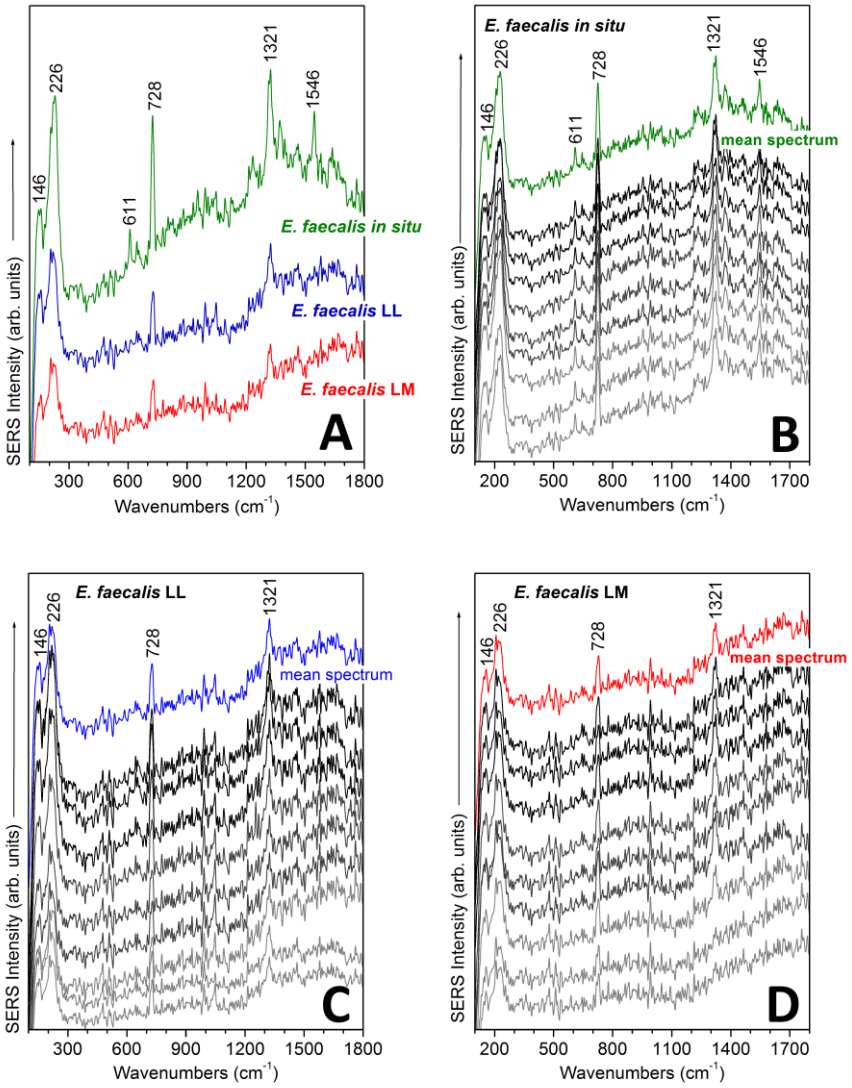

(Color online) Fig. 1 – (A) A comparison between the mean SERS spectra, one for each set of nine recorded data in the three sampling conditions together with full raw spectra for each case: *in situ* (B), LL (C), and LM (D).

These spectral bands are also associated with viability of the bacterial cells as shown by Wang *et al.* [10] when using the 1330/1332 cm^{-1} band as the most intense band for label-free mapping of single bacterial cells by using 785 nm laser line. Live and dead bacteria discrimination was also assessed by Zhou *et al.* using SERS mapping and imaging depending on 730 cm^{-1} and 1330 cm^{-1} intense bands [11]. We consider thus the aforementioned marker SERS as accurate indicators of bacteria detection, independent on the sample preparation protocol used.
In the following, we will exploit the multivariate analysis on the recorded SERS spectra in order to identify unknown sampling protocols applied to *E. faecalis* bacterial cells. We highlight that the reproducible bacterial SERS fingerprint is the main asset in barcoding pathogens, but the herein proposed chemometric analyses offer additional valuable performance to the detection method.

Principal component analysis on full spectrum
The database used for further statistical analyses consists of 27 SERS spectra equally divided for each sample preparation protocol – *E. faecalis* cells mixed with *a priori* synthesized AgNPs obtained from Leopold-Lendl (LL) or Lee Meisel recipe (LM), and *E. faecalis* cells with AgNPs generated *in situ* at their cell wall. Firstly, we performed a *Principal Component Analysis* (PCA) on the *full spectrum* (100 - 1800 cm^{-1}), including 1701 variables (the intensities of each wavenumber). We have calculated 7 PCs. The SERS band at 226 cm^{-1} brings the greatest contribution to the first principal component, present with the highest score on PC-1 loadings plot in Fig. 2. The second greatest contribution comes from 728 cm^{-1} SERS band, while the third, from 146 cm^{-1}. Next, the SERS band at 1321 cm^{-1}, followed by 1546 cm^{-1}, and 611 cm^{-1} bring similar shares. For PC-2, 728 cm^{-1} brings the greatest contribution. The second greatest contribution comes from 146 cm^{-1}, followed by 226 cm^{-1} and 1546 cm^{-1} with equal scores. Smaller contributions come from 611 cm^{-1}, 1321 cm^{-1}, 1370 cm^{-1}, and 1640 cm^{-1} SERS bands, listed in a descending order. Lastly, the main contribution to PC-3 comes from 226 cm^{-1} SERS band, the rest being noise (Fig. 2), an extra reason to consider the first 3 PCs of being sufficient to maximize the variability between samples of different classes, and minimize it between samples within a class; the other reason being the total variance of the first 3 PCs – 98%.

Principal component analysis based on the NP's response
AgNPs specific signal is present in the low frequency area of the SERS spectra with the strongest band 226 cm^{-1} and its shoulder at 146 cm^{-1}. The band at 146 cm^{-1} is assigned to the metallic silver lattice vibrational modes [12], and 226 cm^{-1}, to the Ag-Cl bond when chloride ions might be present in the reagents solution. Also, it might be a band generally attributed to the chemisorbed atomic-molecular oxygen species, when working in open air conditions [12]. This band brings the greatest contribution to all first 3 PCs.

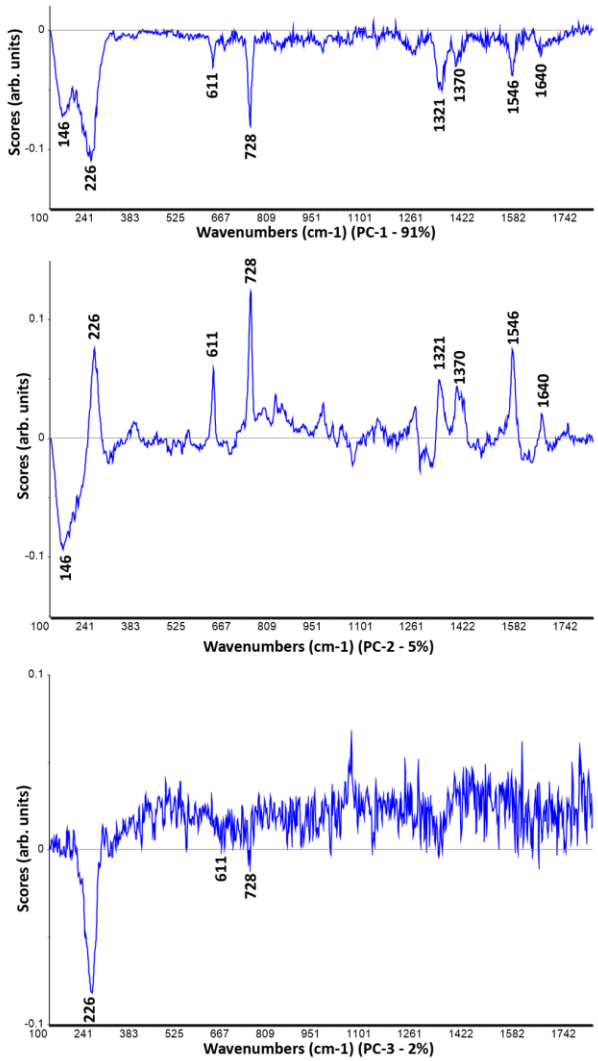

(Color online) Fig. 2 – Loadings plots for PC-1-3 from PCA on full spectral range.

By performing a PCA only on the 100 - 299 cm^{-1} spectral range we expected a dimensionality further reduction of our database. With a total number of only 200 variables, we calculated 7 PCs, out of which the first 2 PCs sum up a total variance of 100%, 96% from PC-1, and 4%, from PC-2.

Principal component analysis of bacterial fingerprint area only

The SERS band at 728 cm^{-1}, assigned to the stretching of glycosidic ring in adenine [8, 13, 14] is of medium to low intensity in the bacterial response of LL and LM protocol, showing a strong sharp band for the sample following the *in situ* protocol.

The only other notable SERS band in LL and LM protocol is 1321 cm^{-1}. This band is assigned to the bending vibration of CH group [10]. It is of medium to low intensity in LL and LM, and strong for *in situ*. Other worth mentioning bands are present just in the *in situ* case - 611 cm^{-1}, assigned to the vibration of COO group in guanine [15, 16], and 1546 cm^{-1}, assigned to stretching of CC groups in combination with bending of NH and CH groups [15]. A PCA was also performed on the *bacterial fingerprint area*, including 1501 variables ranging from 300 – 1800 cm^{-1} (Fig. 3).

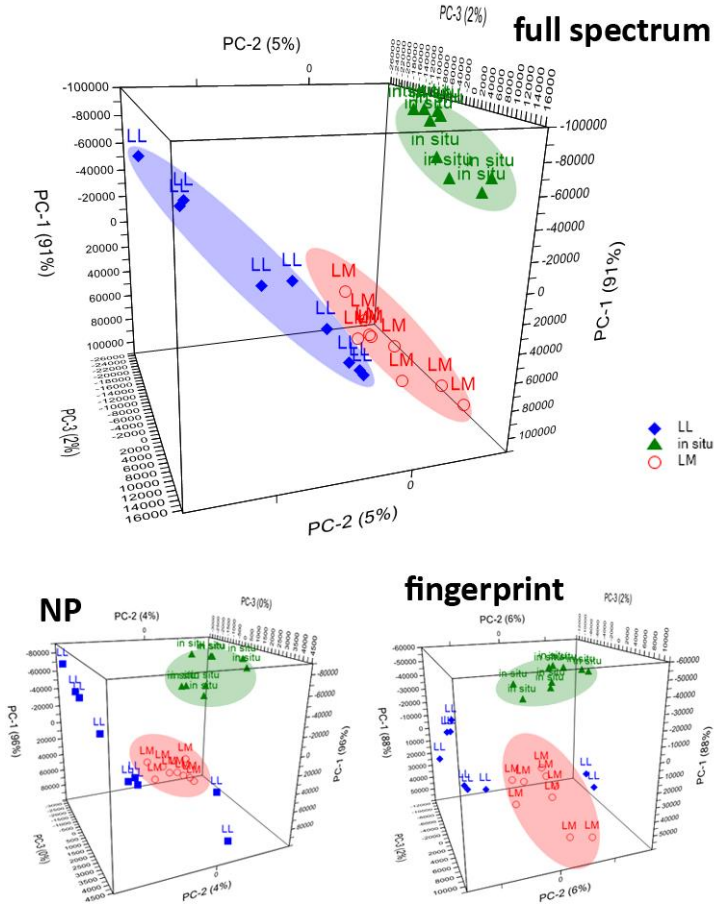

(Color online) Fig. 3 – 3D scores plot of the first 3 PCs of the analysis on full SERS spectra (100 - 1800 cm^{-1}), the AgNPs response (100 – 299 cm^{-1}), and bacterial fingerprint area (300 – 1800 cm^{-1}).

Out of 7 PCs calculated, the total variance for the first three PCs is 96% - 88% (PC-1), 6% (PC-2), and 2% (PC-3). So, by reducing the database by 200 variables, we obtained a similar total variance to the PCA of the full spectral range.

Samples with similar scores on a certain PC cluster together on the scores plot when PCA is used as a classification tool. In the case of PCA on the full spectra, all samples have visibly grouped into three different clusters corresponding to protocol applied (Fig. 3 full spectrum). Clusters do not interfere with each other, the *in situ* group being more compact than the slightly more dispersed LL and LM samples. PC-1 brings a variance of 91% to the total, while PC-2 (5%), and PC-3 (2%) make the separation between LL and LM group more visible.
When PCA was performed on the AgNPs SERS response, we obtained an ideal total variance of 100%. But this is not helpful in the sample grouping, as seen in Fig. 3 NP. *In situ* and LM samples are clustered together, the latter being more compact compared to the classification from PCA on full spectra. But the ideal variance brings two outlying LL samples, dividing the group. We obtained the same clustering scene for PCA on bacterial fingerprint (Fig. 3 fingerprint), LM group being slightly more dispersed.

PCA-LDA

Now that we have identified the spectral differences between the samples subjected to different preparation protocols, we are able to build a classification model for sample grouping labeled as *a priori*, LM and LL protocol, and *in situ* protocol.
The first model contains all 27 SERS spectra with their full spectral range, and uses the first 3 PCs as variables in order to have both as less variables as possible and the greatest variation between the samples. We considered the number of PCs to be sufficient since they sum a total variance of 98%. On the other hand, the contribution to the 4^{th} up to 7^{th} PC is mainly noise (Fig. 2).
Before starting the *linear discriminant analysis*, each sample was labeled as the category it belongs to – LM, LL, and *in situ*. Model I classified correctly all our samples, with a 100% accuracy. As pictured in Fig. 4, the *in situ* SERS signal differs the most from LL signal, since the variation between them based on LD1 is the greatest. Both the *in situ*-LL and *in situ*-LM variations are noticeable and in close ranges on LD2. The same LD2 is the one clearly separating LL from LM samples, no sample interfering with the wrong group.
For a cross validation of the model, we used two thirds of the samples as a training set creating a similar classification model to model I, based on the first 3 PCs. Samples in the training set were *a priori* labeled as the group they belong to. The other third samples were used as the prediction samples. No labels were set for them, and no PC were calculated. This set was assembled by selecting an equal number of three samples from each group. No samples from the test set were used to create the prediction model in order to avoid the over fitting.

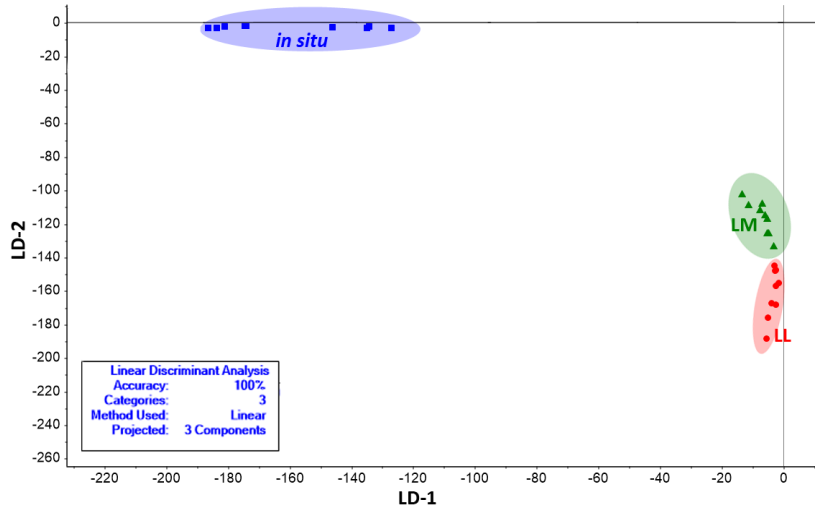

(Color online) Fig. 4 – PCA-LDA discrimination plot for model I.

The selection procedure for the training and testing sets is shown in Table 1. For an accurate validation, we followed the same recipe for 9 models by alternating between the samples used for creating the model and the testing ones. Each of the 9 repetitions is independent from the others. Each model generated a confusion matrix containing the predicted samples and the actual ones.

Table 1

Sample numbers as listed in model I further used as training sets and test sets (**bold**) for model II – X.

Model II	Model III	Model IV	Model V	Model VI	Model VII	Model VIII	Model IX	Model X
LL1	LL1	LL1	LL1	LL1	LL1	LL1	**LL1**	**LL1**
LL2	**LL2**	LL2	LL2	LL2	LL2	LL2	LL2	**LL2**
LL3	**LL3**	**LL3**	LL3	LL3	LL3	LL3	LL3	LL3
LL4	**LL4**	**LL4**	**LL4**	LL4	LL4	LL4	LL4	LL4
LL5	LL5	**LL5**	**LL5**	**LL5**	LL5	LL5	LL5	LL5
LL6	LL6	LL6	**LL6**	**LL6**	**LL6**	LL6	LL6	LL6
LL7	LL7	LL7	LL7	**LL7**	**LL7**	**LL7**	LL7	LL7
LL8	LL8	LL8	LL8	LL8	**LL8**	**LL8**	**LL8**	LL8
LL9	LL9	LL9	LL9	LL9	LL9	**LL9**	**LL9**	**LL9**
in situ1	in situ1	in situ1	in situ1	in situ1	in situ1	in situ1	**in situ1**	**in situ1**
in situ2	**in situ2**	in situ2	in situ2	in situ2	in situ2	in situ2	in situ2	**in situ2**
in situ3	**in situ3**	**in situ3**	in situ3	in situ3	in situ3	in situ3	in situ3	in situ3
in situ4	**in situ4**	**in situ4**	**in situ4**	in situ4	in situ4	in situ4	in situ4	in situ4
in situ5	in situ5	**in situ5**	**in situ5**	**in situ5**	in situ5	in situ5	in situ5	in situ5
in situ6	in situ6	in situ6	**in situ6**	**in situ6**	**in situ6**	in situ6	in situ6	in situ6
in situ7	in situ7	in situ7	in situ7	**in situ7**	**in situ7**	**in situ7**	in situ7	in situ7
in situ8	in situ8	in situ8	in situ8	in situ8	**in situ8**	**in situ8**	**in situ8**	in situ8
in situ9	in situ9	in situ9	in situ9	in situ9	in situ9	**in situ9**	**in situ9**	**in situ9**
LM1	LM1	LM1	LM1	LM1	LM1	LM1	**LM1**	**LM1**
LM2	**LM2**	LM2	LM2	LM2	LM2	LM2	LM2	**LM2**
LM3	**LM3**	**LM3**	LM3	LM3	LM3	LM3	LM3	LM3

LM4	**LM4**	**LM4**	**LM4**	LM4	LM4	LM4	LM4	LM4
LM5	LM5	**LM5**	**LM5**	**LM5**	LM5	LM5	LM5	LM5
LM6	LM6	LM6	**LM6**	**LM6**	**LM6**	LM6	LM6	LM6
LM7	LM7	LM7	LM7	**LM7**	**LM7**	**LM7**	LM7	LM7
LM8	LM8	LM8	LM8	LM8	**LM8**	**LM8**	**LM8**	LM8
LM9	LM9	LM9	LM9	LM9	LM9	**LM9**	**LM9**	**LM9**

In order to evaluate the net performance of our classification model, we have calculated several *key performance indicators (KPI)* for each model: *accuracy*, *precision*, *sensitivity*, and *specificity* [17]. Their values are listed in Table 2, both for the training and testing sets.

Table 2

KPI for model II-X on both training (TR) and testing (TE) sets; A – accuracy, P – precision, Sens – sensitivity; Sp – specificity; all values are in percentages (%).

Model	**A_{TR}**	**A_{TE}**	**P_{TR}**	**P_{TE}**	**$Sens_{TR}$**	**$Sens_{TE}$**	**Sp_{TR}**	**Sp_{TE}**
II	100	100	100	100	100	100	100	100
III	100	100	100	100	100	100	100	100
IV	100	100	100	100	100	100	100	100
V	100	100	100	100	100	100	100	100
VI	94.45	77.78	100	86.67	94.45	77.78	97.22	88.89
VII	100	100	100	100	100	100	100	100
VIII	100	77.78	100	86.67	100	77.78	100	88.89
IX	100	100	100	100	100	100	100	100
X	100	100	100	100	100	100	100	100
Range	94.45-100	77.78-100	100	86.67-100	94.45-100	77.78-100	97.22-100	88.89-100
Average	**99.38**	**95.06**	**100**	**97.04**	**99.38**	**95.06**	**99.69**	**97.53**

Our classification model is described on average by an accuracy and sensitivity of over 95%, while its precision and specificity are over 97%. All training sets scored 100% accuracy except model VI where sample LL1 was predicted as being LM. The same model scores lower KPIs for its test set, two LL samples (LL6 and LL7) being falsely predicted as LM. For model VIII's test set – samples LL8 and LL9 were falsely predicted as being LM, even if the training set predicted correctly all sample. The average KPIs values indicate that a cross validation is necessary when creating a prediction model otherwise its prediction potential will be specific only to the particular samples used. On the other hand, characterizing a prediction model only by its accuracy is not enough since the model might present lower values for other statistical indicators.

5. CONCLUSIONS

Our prediction model designed by using PCA-LDA is able to distinguish between the three sample preparation protocols, *a priori* LL and LM, and *in situ* with an overall accuracy and sensibility of 95%, and an average precision and specificity of 97%. We consider the obtained results as an indicator of the high potential of using

such user-friendly multivariate analysis, usually already implemented in the software of the spectrometer, for a reliable and fast analysis with further clinical use.

Acknowledgements. Financial support from the Romanian Ministry of Education, CCCDI-UEFISCDI, project number PN-III-P1-1.1-TE-2019-0910 within PNCDI III, is highly acknowledged. The authors gratefully appreciate the help of PhD Tiberiu Szöke-Nagy from National Institute for Research and Development of Isotopic and Molecular Technologies, Molecular and Biomolecular Physics Department for providing the bacterial biomass in standardized samples.

REFERENCES

1. N. Leopold, *Surface-enhanced Raman Spectroscopy: Selected Applications*, Napoca Star, 2009.
2. M. Moskovits, J. Raman Spectrosc., **36**, 485-496 (2005).
3. K. J. Ryan and C. G. Ray, *Sherris Medical Microbiology*, 2004.
4. O. Alfakhrany, A. Aziz, T. El-Banna and F. Sonbol, J. Clin. Cell. Immunol., **9** (5), 1-9 (2018).
5. H. Zhou, D. Yang, N. P. Ivleva, N. E. Mircescu, R. Niessner and C. Haisch, Anal. Chem., **86**, 1525-1533 (2014).
6. N. Leopold and B. Lendl, J. Phys. Chem. B, **107** (2003).
7. P. C. Lee and D. Meisel, J.Phys. Chem., **86**, 3391-3395 (1982).
8. P. Kubryk, R. Niessner and N. P. Ivleva, Analyst, **141**, 2874-2878 (2016).
9. W. R. Premasiri, J. C. Lee, A. Sauer-Budge, R. Théberge, C. E. Costello and L. D. Ziegler, Anal. Bioanal. Chem., **408**, 4631-4647 (2016).
10. P. Wang, S. Pang, J. Chen, L. McLandsborough, S. R. Nugen, M. Fan and L. He, Analyst, **141**, 1356-1362 (2016).
11. H. Zhou, D. Yang, N. P. Ivleva, N. E. Mircescu, S. Schubert, R. Niessner, A. Wieser and C. Haisch, Anal. Chem., **87**, 6553-6561 (2015).
12. I. Martina, R. Wiesinger, D. Jembrih-Simbuerger and M. Schreiner, e-Preservation Science, **9**, 1-8 (2012).
13. N. P. Ivleva, M. Wagner, A. Szkola, H. Horn, R. Niessner and C. Haisch, J. Phys. Chem. B, **114**, 10184-10194 (2010).
14. A. Walter, A. März, W. Schumacher, P. Rösch and J. Popp, Lab. Chip, **11**, 1013-1021 (2011).
15. M. Kahraman, M. M. Yazıcı, F. Şahin and M. Çulha, Langmuir, **24**, 894-901 (2008).
16. M. Knauer, N. P. Ivleva, X. Liu, R. Niessner and C. Haisch, Anal. Chem., **82**, 2766-2772 (2010).
17. C. Beleites, R. Salzer and V. Sergo, Chemom. Intell. Lab. Syst., **122**, 12-22 (2013).